Production of PbS by the method of chemical bath deposition at relatively low solution temperatures

B. ALTIOKKA*, M. ONAL*
Bilecik Seyh Edebali University, Bilecik, 11000, Turkey

As the aim of this study, we produced PbS thin films by the chemical bath deposition method. While producing the films, the solution temperatures were reduced from 20 °C down to 0 °C. According to XRD patterns, it was observed that all the films had galena-type cubical crystal structures. In addition, it was found that the crystallite sizes increased depending on the increasing solution temperatures. When the morphologies of the film surfaces were examined with the SEM device, it was seen that the film produced at 10 °C was pinhole-free. According to the SEM images, it was noticed that the surface roughness of the films obtained at 0, 5, and 10 °C was higher than that of the other samples. The film photo showed that all films were deposited onto the glass surface tightly.

(Received July 20, 2022; accepted February 14, 2023)

Keywords: PbS, Chemical bath deposition, Thin film, Low temperature

1. Introduction

All IV-VI group semiconductor materials including lead sulfide in particular have been of interest to researchers for many years due to their wide application possibilities in the optoelectronic and photovoltaic industries [1-3]. PbS thin film bandgap values can change between 0.41 eV and 2.3 eV depending on the crystallite size [4]. PbS semiconductor possesses unique electronic properties. Lead sulfide has high permeability (εPbS = 15-20') and the absorption coefficient in the spectral regions of visible light and near-infrared (IR) corresponds to a high value of ~10^5 cm^{-1} [5]. Used extensively in sensors and optoelectronic devices as materials for infrared detectors, PbS thin films have also been preferred for solar energy converters and optical switches as well as chemical, temperature and flame sensors [6]. Researchers have used many deposition methods for depositing PbS thin films on glass substrates. Some of these methods include electrodeposition, spray pyrolysis, SILAR method, chemical bath deposition [7], chemical vapor deposition and thermal evaporation [8]. The CBD method is widely used because it does not require complex instruments like vacuum systems and similar costly equipment. The basic equipment has a hot plate and a magnetic stirrer. Also, the initial chemicals are usually accessible and affordable. CBD stands out among other methods due to its simplicity and inexpensiveness in addition to its convenience in depositing to larger areas [9].

When producing lead sulfide films by the CBD method, the reaction steps are given below [10];

$$Pb(NO_3)_2 + 2NaO \rightarrow Pb(OH)_2 + 2NaNO_3 \quad (1)$$

$$Pb(OH)_2 + 4NaOH \rightarrow Na_4Pb(OH)_6 \quad (2)$$

$$Na_4Pb(OH)_6 \rightarrow 4Na^+ + HPbO^-_2 + 3OH + H_2O \quad (3)$$

$$SC(NH_2)_2 + OH^- \rightarrow CH_2N_2 + H_2O + SH^- \quad (4)$$

$$HPbO^-_2 + SH^- \rightarrow PbS + 2OH^- \quad (5)$$

During the present study, PbS thin films were grown by means of CBD and the effects of relatively low temperature were investigated in detail. So far, PbS thin films have been produced at the solution temperature of the lowest 15°C [11]. However, solution temperature was not investigated and only delay time was investigated in the mentioned study. In our study, the solution temperature was reduced from 20 °C down to 0 °C at 5 °C intervals. Therefore, it can be said that PbS thin films were produced at solution temperatures of 0, 5, and 10 °C for the first time. This study is important because of the fact that pinhole-free samples were obtained at only 10 °C and surface roughness was seen as relatively high. These values are quite favorable for solar cells.

2. Experimental details

The CBD method was employed for the PbS precipitation process onto glass substrates. The bath container and glass substrates washed with acetone were rinsed with distilled water before the deposition process. And the final solution was prepared using 0.282 g of $Pb(NO_3)_2$, 0.58 g of NaOH and 0.388 thiourea compounds. For final solutions, 100 ml of deionized water was used. The solution pH value was measured as approximately 10.0 for all samples. The deposition process for all samples was completed in 75 minutes. All solutions were stirred at 600 rpm. The solution temperatures were kept at 0, 5, 10, 15, and 20 °C using ice blocks. The experimental conditions are submitted in Table 1. Subsequent to the deposition process, the samples were rinsed with pressurized deionized water and dried under room

conditions. The samples were labeled as C0, C1, C2, C3, and C4, respectively, according to the bath temperatures of 0, 5, 10, 15, and 20 °C. The gravimetric method was used to calculate the film thicknesses. PANalytical Empyrean XRD diffractometer was utilized in 2θ angles ranging between 20° and 70° for the X-ray diffraction study of the deposited PbS thin films. APERKIN Elmer FTIR device was used for Fourier transform analysis. PbS films' surface morphology was studied using a Zeiss SUPRA 40VP scanning electron microscope (SEM). Surface roughness values were calculated using ImageJ software and SEM images.

Table 1. Experimental conditions for chemically deposited PbS

Expt.	$Pb(NO_3)_2$ (g)	NaOH (g)	Thiourea Total(g)	Temp. (°C)	Dep. Time (min)
C0	0.282	0.58	0.388	0	75
C1	0.282	0.58	0.388	5	75
C2	0.282	0.58	0.388	10	75
C3	0.282	0.58	0.388	15	75
C4	0.282	0.58	0.388	20	75

3. Results and discussion

3.1. Structural analysis for PbS films

The film thicknesses were achieved by the gravimetric method given in Eq. (6) and they were measured at approximately 600 nm for all samples.

$$t = \frac{m}{\rho A} \tag{6}$$

In this equation, t indicates the film thickness, m indicates the mass of the film, ρ indicates the density, and A indicates the surface area. The bulk sample density for PbS is 7.59 g/cm^3 [12].

XRD patterns were presented in Fig. 1. In Fig. 1, all of the films are seen in a galena-type cubical structure. It is fully compatible with the ASTM card numbered 98-003-8293. In the literature, we found that the solution temperatures at which PbS thin films are mostly produced were 15-45 °C [13- 17]. In our study, as seen in Fig. 1, the XRD peak intensities of the film produced at 20°C were lower than that of the others. In a previous study, it was reported that the reaction rate was highly effective on XRD peak intensities [18].

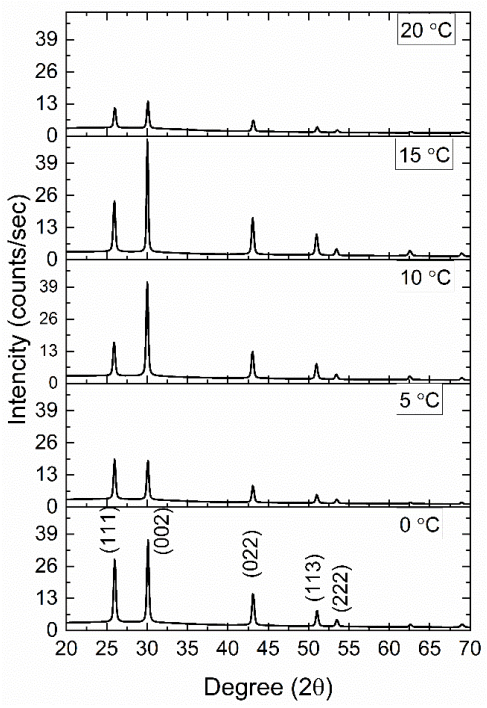

Fig. 1. XRD patterns for PbS thin films

The texture coefficient was calculated using Eq. (7) to determine the crystal orientation [19].

$$TC = \frac{I_{(hkl)}/I_{0(hkl)}}{\frac{1}{N}\sum_N \left(\frac{I_{(hkl)}}{I_{0(hkl)}}\right)} \tag{7}$$

where $I_{0(hkl)}$ and $I_{(hkl)}$ indicate the standard X-ray intensity of the PbS films and the measured X-ray intensity, whereas N indicates the reflection number. The TC values are given in Table 2. According to Table 2, the TC values of the films obtained at 10 and 15 °C were relatively denser in the (002) plane.

Table 2. Texture coefficient of PbS thin films

hkl	C0	C1	C2	C3	C4
(111)	1.05	1.75	0.66	0.69	1.02
(002)	1.20	1.10	1.61	1.63	1.21
(022)	0.75	0.72	0.72	0.68	0.77

The Debye Scherrer equation given in Eq. (8) was used for calculating the crystallite size values of the films. The calculation results are given in Table 3.

Table 3. Crystallite sizes of PbS films

Expt.	cs (nm) (111)	cs (nm) (002)	cs (nm) (022)	cs (nm) Average
C0(0 °C)	50	42	35	42
C1(5 °C)	42	46	38	42
C2(10 °C)	49	42	38	43
C3(15 °C)	53	50	44	49
C4(20 °C)	48	67	38	51

For calculation of full width half maximum (FWHM), the origin pro software was used.

$$cs = \frac{0.089*180*\lambda}{314*\beta*\cos\theta_C} nm \quad (8)$$

where λ indicates the wavelength of X-ray radiation (1.54056 Å), β indicates the full width half maximum, $2\theta_C$ indicates the peak center [20]. Crystallite size values increased from 42 nm to 51 nm depending on the temperature increase. This was an expected result. Because, as the solution temperature increases, the reaction rate increases, and it is expected to increase the crystal size.

The corrected values of lattice constants given in Fig. 2 were estimated from the Nelson–Reilly plots. The Nelson-Riley curve was plotted between the lattice constant 'a' and the error function calculated for different planes. In Eq. (8), the function used to calculate the lattice constants is given below [21].

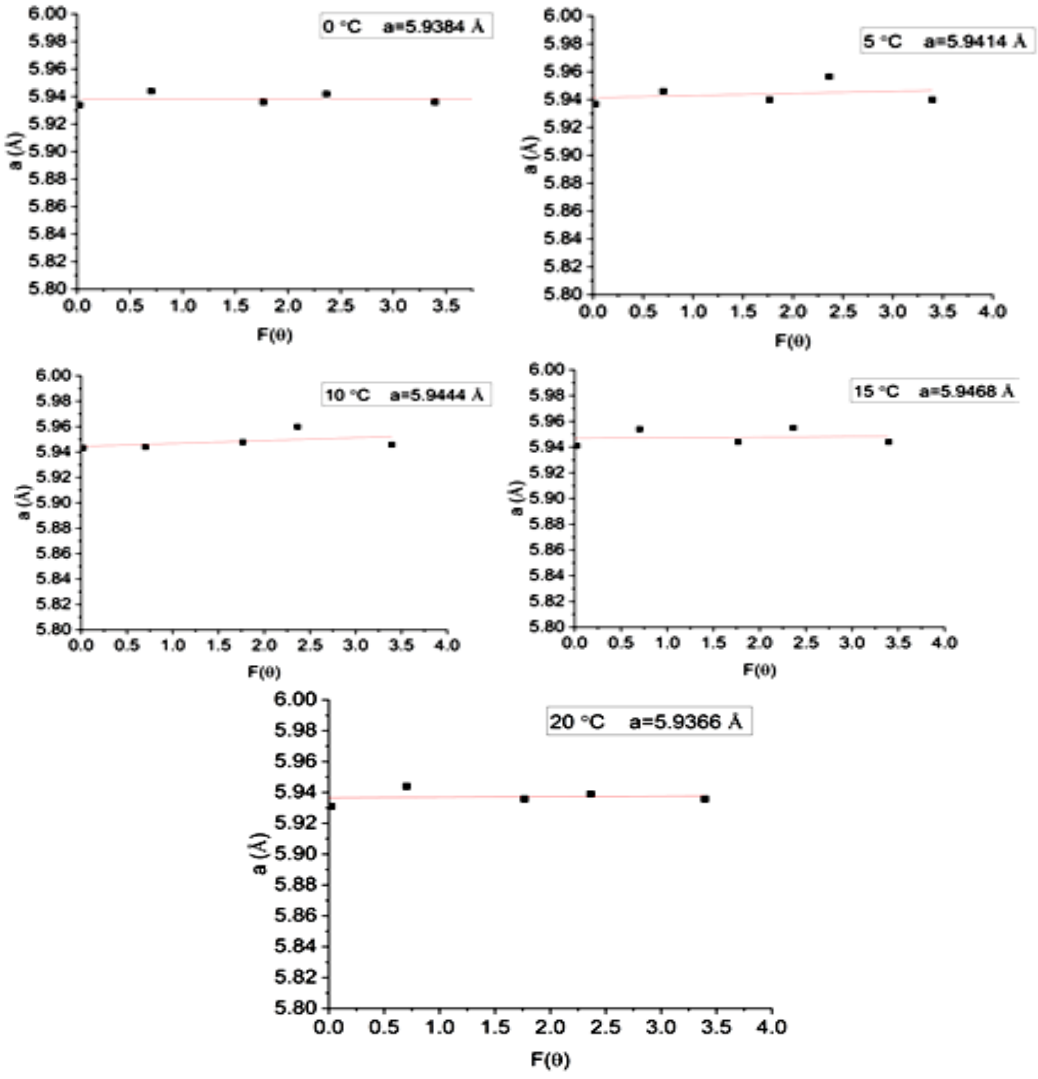

Fig. 2. Nelson Riley plots for C0, C1, C2, C3, and C4

$$F_{(\theta)} = \frac{1}{2}\left(\frac{\cos^2\theta}{\sin\theta} + \frac{\cos^2\theta}{\theta}\right) \quad (9)$$

The adjusted 'a' value was obtained by estimating for plot θ =90°. According to the Nelson Riley plots, the lattice constant of all the produced films was higher than the lattice constant of the bulk sample. These corrected lattice values showed that the films were under stress.

The dislocation density (δ) represents the length of the dislocation lines per unit volume of the crystal. Small values mean that the crystallization level of the sample is good. Dislocation density was calculated with Eq. (10) [22] and given in Table 4.

$$\delta = \frac{1}{(cs)^2} \quad (10)$$

Table 4. Dislocation density and lattice constant

Expt.	Lattice Constant for bulk sample	Lattice Constant (corrected) from Nelson Riley	Dislocation Density (lines/m2)* 1014
C0	5.934	5.938	0.566
C1	5.934	5.941	0.566
C2	5.934	5.944	0.540
C3	5.934	5.946	0.416
C4	5.934	5.936	0.384

3.2. FTIR for the PbS films

FTIR spectroscopy was used to analyze the chemical bonds present in the produced PbS thin films. FTIR spectrum analysis of PbS samples was performed in different frequency regions ranging from 400 to 4000 cm-1. FTIR spectra of PbS thin films are shown in Fig. 3. Metal oxides normally present absorption bands under 1000 cm^{-1}, which are caused by interatomic vibrations in the fingerprint region [23]. While the vibrations seen at 760 cm^{-1} and 900 cm^{-1} are thought to be related to metal oxide bonds, the peaks between 420 cm^{-1} and 450 cm^{-1} indicate weak and moderate PbS bonds [24-25]. Because of the fact that the Pb-S bond is basically an electrovalent bond, the FTIR spectra of PbS do not display strong bands related with Pb–S stretching and bending vibrations [26]. According to the FTIR plots, as the temperature increased, the PbS thin film transmittance decreased in the wavelength range of 1000-4000 cm^{-1}.

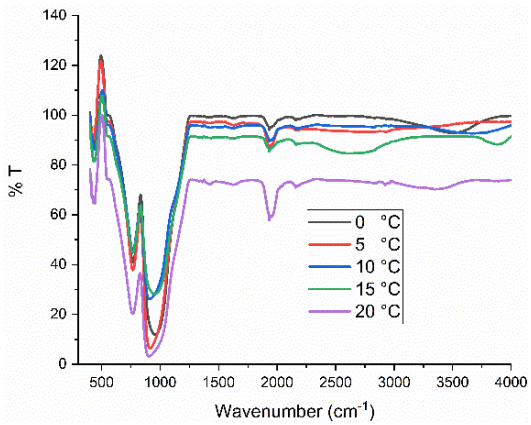

Fig. 3. Wavenumber versus FTIR spectra for PbS films

3.3. SEM analysis for the PbS films

The surface morphologies of the samples were analyzed from SEM images.

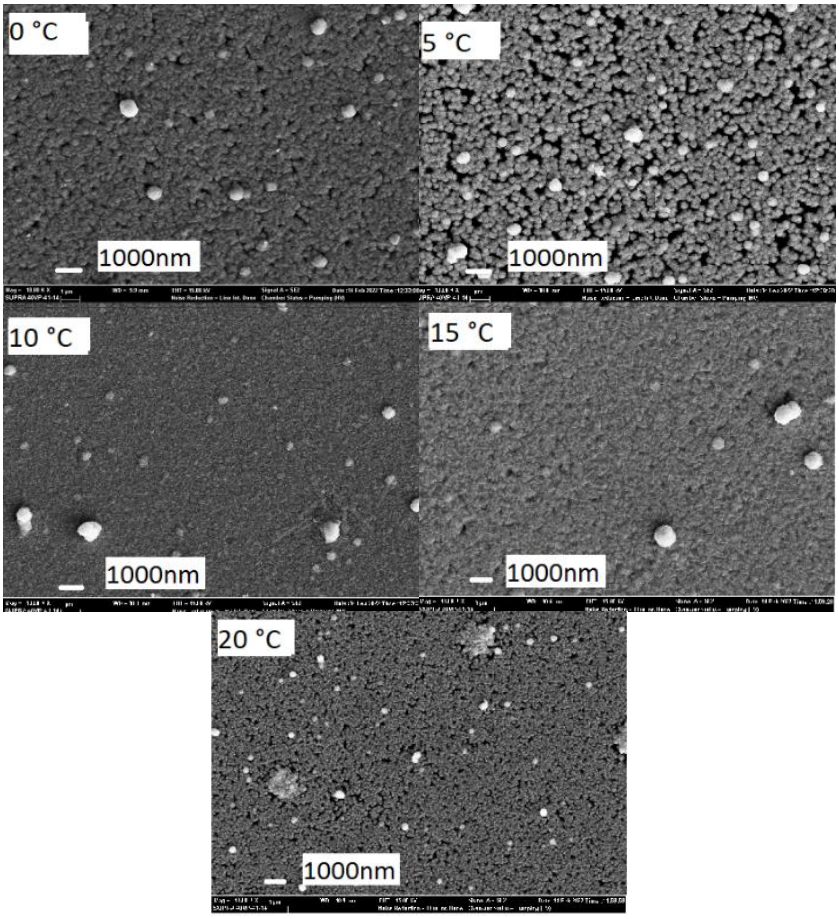

Fig. 4. SEM images of PbS thin films magnified 10000 times

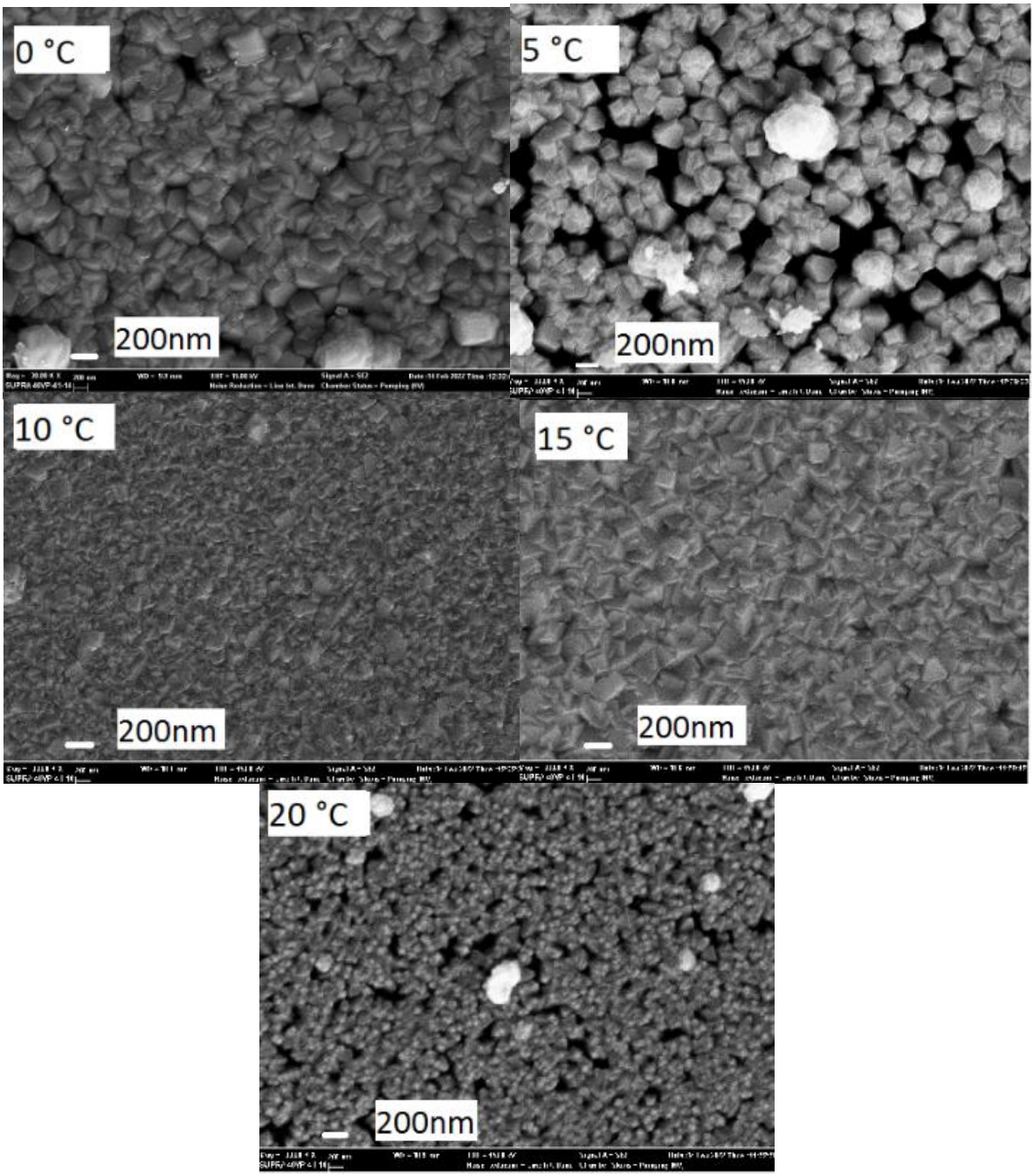

Fig. 5. SEM images of PbS thin films magnified 30000 times

Fig. 4 presents SEM images of the samples at 10000 times magnification. There were no pinholes and voids on the film that was produced only at 10 °C. This was a very important result. Because no film had been produced at 10 °C before in the literature. SEM images of the films magnified 30000 times are given in Fig. 5. When Fig. 5 is examined, no pinhole was found on the film produced only at 10 °C, as in Fig. 4. On the other hand, there were gaps and pinholes on the surfaces of the films obtained at 0, 5, 15 and 20 °C.

SEM images were processed using ImageJ software to detect the surface roughness of the samples. Surface roughness values calculated as average (Ra) and root mean square (Rq) are presented in Table 5 and surface roughness images obtained using ImageJ software are presented in Fig. 6.

Table 5. Surface roughness values calculated with ImageJ software

Expt.	Temp. (°C)	ra (nm)	rq(nm)
C0	0	22	27
C1	5	21	26
C2	10	12	16
C3	15	9	12
C4	20	11	14

When Table 5 is examined, it can be seen that the surface roughness values decrease from 22 nm to 11 nm depending on the solution temperature increase. This result was important for solar cells. Because the increase in surface roughness means an increase in the surface area and therefore an increase in photon absorption.

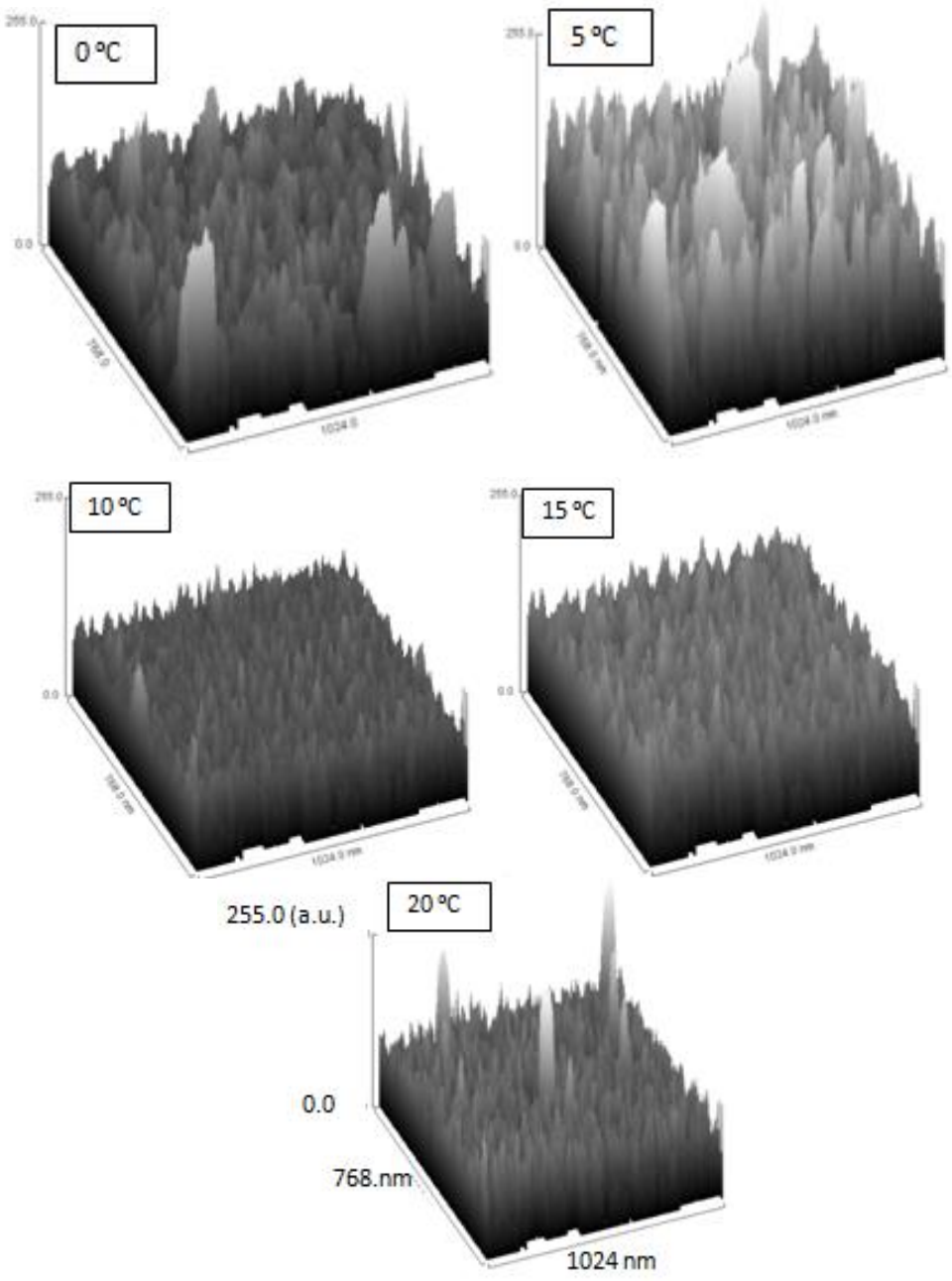

Fig. 6. Surface roughness plots of PbS thin films

3.4. Visual photo for the PbS films

The photo of the films was taken from top view of the surfaces and the photo is given in Fig. 7. Fig. 7 shows that the films adhered well onto the glass substrates.

On the surfaces of the films, cracks and voids were not seen. The surfaces were very compact. Besides, there was only a tonal difference on the surface. It was concluded that tonal difference was sourced crystallite size.

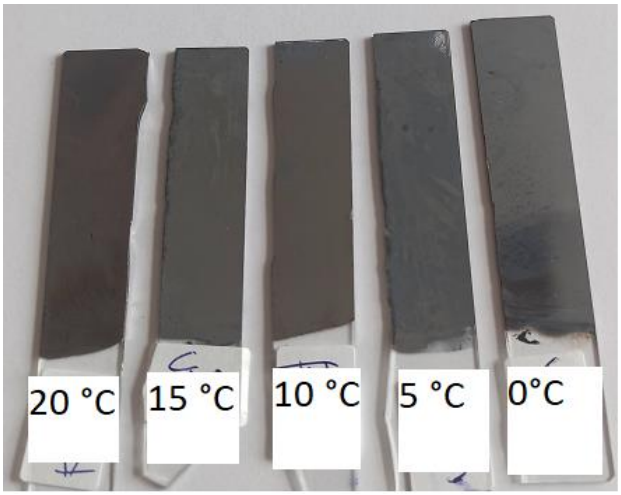

Fig. 7. Photograph of PbS films

4. Conclusions

In this study, the PbS films were deposited onto glass substrates by using chemical bath deposition. Besides, results of relatively cold solutions were investigated in detail. The temperatures were chosen as to be 0, 5, 10, 15 and 20 °C. The XRD patterns showed that all films were grown cubical structure. The crystallite sizes were increased from 42 to 51 nm depending on increasing temperature. Surface properties were analyzed from SEM images. As seen in SEM images, there were no voids and pinholes on the film surface obtained at only 10 °C. This result was ideal for solar cells and other devices. As the temperature of the solutions decreased, the surface roughness increased. This result was also ideal for solar cell because of the fact that increasing surface roughness caused a large surface area. FTIR transmission spectra of the PbS thin film was noted in the wavenumber range of 400–4000 cm^{-1}. According to the FTIR plots, as the temperature increased, the PbS thin film transmittance decreased. As a result, the film produced at 10 °C was found to be quite suitable for solar cells and other optoelectronic devices according to the XRD and SEM analysis results.

References

[1] Z. I. Smirnova, V. M. Bakanov, L. N. Maskaeva, V. F. Markov, V. I. Voronin, Phys. Solid State **56**, 2561 (2014).
[2] A. S. Obaid, M. A. Mahdi, Z. Hassan, M. Bououdina, Mater. Sci. Semicond. Process **15**, 564 (2012).
[3] N. B. Kotadiya, A. J. Kothari, D. Tiwari, T. K. Chaudhuri, Appl. Phys. A Mater. Sci. Process **108**, 819 (2012).
[4] F. Göde, F. Yavuz, I. A. Kariperb, Acta Phys. Pol. A **128**, 215 (2015).
[5] L. N. Maskaeva, E. V. Mostovshchikova, V. I. Voronin, A. V. Pozdin, I. O. Selyanin, I. A. Anokhina, V. F. Markov, Semiconductors **55**, 855 (2021).
[6] L. N. Maskaeva, E. V. Mostovshchikova, V. F. Markov, V. I. Voronin, A. V Pozdin, I. O. Selyanin, A. I. Mikhailova, Semiconductors **56,** 1049 (2022).
[7] A. El Madani, O. D. S. Benyoussef, A. Q. M. Fahoume, Brazilian J. Phys **51**, 1166 (2021).
[8] A. S. Obaid, M. A. Mahdi, Z. Hassan, M. Bououdina, Int. J. Hydrogen Energy **38**, 807 (2013).
[9] G. Geetha, P. Murugasen, S. Sagadevan, Acta Phys. Pol. A **132**, 1221 (2017).
[10] B. Altiokka A. K. Yildirim, J. Optoelectron. Adv. M. **21**(9-10), 623 (2019).
[11] M. Önal B. Altıokka, J. Nano Res **63,** 1 (2020).
[12] F. Göde S. Ünlü, Mater. Sci. Semicond. Process **90**, 92 (2019).
[13] B. Abdallah, A. Ismail, H. Kashoua, W. Zetoun, J. Nanomater. **2018**, 1 (2018).
[14] E. Yücel, Y. Yücel, B. Beleli, J. Alloys Compd **642**, 63 (2015).
[15] M. Önal B. Altıokka, J. Nano Res. **63**, 1 (2020).
[16] K. V. Khot, S. S. Mali, N. B Pawar, R. M. Mane, V. V. Kondalkar, V. B. Ghanwat, P. N. Bhosale, Journal of Materials Science: Materials in Electronics **25**, 3762 (2014).
[17] J. Yang A. V. Walker, Langmuir **30**, 6954 (2014).
[18] B. Altiokka, M. C. Baykul, M. R. Altiokka, J. Cryst. Growth **384**, 50 (2013).
[19] M. Alaf, M. O. Guler, D. Gultekin, H. Akbulut, Acta Phys. Pol. A **123**, 326 (2013).
[20] M. Önal B. Altıokka, Crystallogr. Reports **65**, 1237 (2020).
[21] A. Hussain, A. Begum, A. Rahman, Arab. J. Sci. Eng **38**, 169 (2013).
[22] S. Temel, M. Nebi, D. Peker, Gazi Üniversitesi Fen Bilimleri Dergisi Part C: Tasarım ve Teknoloji **5**, 51 (2017).
[23] H. Kumar, R. Rani, International Letters of Chemistry, Physics and Astronomy **14**, 26 (2013).
[24] S. Sharma, A. V. D. Reddy, N. Jayarambabu, N. V. M. Kumar, A. Saineetha, S. Kailasa, K. Rao, Mater. Today Proc. **26**, 162 (2020).
[25] S. Rajathi, K. Kirubavathi, K. Selvaraju, Arab. J. Chem. **10**, 1167 (2017).
[26] S. B. Pawar, J. S. Shaikh, R. S. Devan, Y. R. Ma, D. Haranath, P. N. Bhosale, P. S. Patil, Applied Surface Science **258**, 1869 (2011).

* Corresponding authors: baris.altiokka@bilecik.edu.tr; metehan.onal@bilecik.edu.tr